expressed on the developing [38] and adult [39] cerebellar granule cells. Furthermore, contrary to the neurotoxic effects of glutamate, NMDA receptors were found to promote the survival of cultured Purkinje [40] and granule cells [41,42]. However, double-KO mice with disrupted *Nr2A* and *Nr2C* genes (encoding two major NMDA receptor subunits in the adult mice cerebellum) demonstrate a mild impairment in motor coordination, but they do not exhibit an ataxic phenotype [43]. This observation suggests that NMDA receptors and GRID2 functions may not be directly linked [44].

Thus, in the present study, pharmaco-behavioral approaches failed to identify *Grid2* as a candidate for the cause of the observed phenotypes. Unexpectedly, our efforts resulted in the observation of new phenotypes in our *Grid2* deficient mice, which appeared as enhanced memantine susceptibility, which was likely mediated by dysfunctional NMDA receptors [1,2,45]. OKR measurements in $Grid2^{Htake/Htake}$ mice revealed impaired basal cerebellar functions in eye movement, which was also mimicked by memantine treatment. Dizziness has been reported as a major adverse effect of memantine treatment in humans [6,46]. The cerebellar flocculus is thought to be responsible for the early stage formation of OKR adaptation and its memory [47,48].

The *Grid2* gene is located in a hot spot of genomic deletions [31], and a number of mutant lines with defects in this gene have been identified. In addition to naturally occurring mutants, targeted disruption and knock-in mutations of *Grid2* have been reported [30,49,50]. In contrast to these loss-of-function mutations, $Grid2^{Lc}$ (*Lurcher*) [51] was identified as a spontaneous dominant mutation characterized by cerebellar ataxia and atrophy of Purkinje and granule cells [30]. Physiological studies of $Grid2^{Lc/+}$ mice have shown that the $Grid2^{Lc}$ mutation produces constitutive inward Ca^{2+}/Na^{+} currents that induce cell death [52].

The importance of the genetic background on $Grid2^{Lc/+}$ mice phenotypes was also reported [47,53]. In congenic $Grid2^{Lc/+}$ mice, almost 99.99% of those on a C57BL/6 genetic background lost Purkinje cells, whereas no Purkinje cell loss was observed in $Grid2^{Lc/+}$ mice on a 93% C57BL/6 genetic background, indicating that phenotypes in $Grid2^{Lc/+}$ mice are highly dependent on their genetic backgrounds. Interestingly, abnormal eye-movement and impaired motor-coordination were only observed in 93% of C57BL/6 background-$Grid2^{Lc/+}$ mice possessing Purkinje cells, but not in 99.99% of C57BL/6 background-$Grid2^{Lc/+}$ mice without Purkinje cells [47], suggesting that gain of GRID2 signaling is also a cause of motor deficits in the presence of Purkinje cells. In contrast to $Grid2^{Lc/+}$ mice, we noticed during gene mapping that memantine-induced balance impairment was observed in $Grid2^{Htake/Htake}$ mice irrespective of their genetic backgrounds (mixed B6 and C3 backgrounds). This is also the case for random eye movements commonly observed in different *Grid2*-deleted mice with different genetic backgrounds, *Grid2*-KO in C57BL/6 and $Grid2^{ho\text{-}15J/15J}$ on a C3HJ background [17], suggested that memantine-induced balance impairment may occur in other *Grid2* deficient mice irrespective of their genetic backgrounds.

How does the $Grid2^{Htake}$ deletion enhance the actions of memantine? GRID2 regulates long-term depression (LTD) at synapses between immature parallel fibers and Purkinje cells by inducing AMPA receptor endocytosis [34,35]. D-Serine is an endogenous ligand for GRID2 and one of the factors that induce LTD [9]. Developing mice that express GRID2 with a disrupted D-serine binding site show impaired motor coordination and learning, suggesting the importance of LTD for motor regulation. On the other hand, NMDA receptor activation requires the removal of Mg^{2+} block, which occurs when the membrane potential increases through activation of non-NMDA receptors including AMPA receptors [4].

Cooperative signal-transmission from cerebellar mossy fiber-granule cells to Purkinje cells mediated by NMDA and AMPA receptors has been shown in both Mg^{2+} block dependent and independent manners [54]. We observed that co-treatment with memantine and AMPA impaired gait and OKR in wild type mice, suggesting that dysregulation of AMPA receptor function in *Grid2* deficient mice may cause the enhanced memantine susceptibility. This may be implicated in the decreased number of memantine-sensitive NMDA-responsible granule cells in *Grid2*$^{Htake/Htake}$ mice.

Whilst mapping the gene responsible for the ataxic phenotype, we observed new phenotypes in *Grid2* deficient mice, which were latent balance defects, and OKR impairments. These deficits were also mimicked by memantine with AMPA in the impaired WT mice. Because, recently, the wide distributions of *Grid2* mRNA and GRID2 protein were reported in the adult rodent brain [55], the phenotypes in *Grid2*$^{Htake/Htake}$ mice could be ascribed to not only attenuated NMDA receptor responsiveness in a subset of granule cells but also other cellular mechanisms.

When granule cells are collectively activated *in vivo*, glutamate spilt over from parallel fiber-Purkinje cell synapses stimulate adjacent interneurons (volume transmission), which in turn exert inhibition of Purkinje cells [44,56–58] crucial for normal motor coordination [59]. The GRID2 mutation may reduce NMDA receptor-mediated excitation of granule cells, and this might decrease the volume transmission and Purkinje cell inhibition via interneurons. Moreover, cerebellar interneurons (basket, stellate, and Golgi cells) also express functional NMDA receptors at their presynaptic membrane [44,56–58] and these receptors could be affected by the change of GRID2 signaling. Taken as a whole, the present study using a naturally occurring *Grid2* deleted mouse line may lead to a better understanding of NMDA, AMPA, and GRID2 receptors. Further studies are required to elucidate the precise mechanisms underlying GRID2 signaling.

4. Experimental Section

4.1. Animals

C57BL/6J (B6) and C3H/HeN (C3) from SLC Japan (Shizuoka, JAPAN) were used for the maintenance of the *Grid2*$^{Htake/Htake}$ mouse line and for IVF for microsatellite analyses, respectively. IVF was performed following a standard method [60] using human tubal fluid medium (Ark Resource, Kumamoto, Japan). The *Grid2* mutant mice, *Grid2*$^{Htake/Htake}$ (formal name is *Grid2*$^{ho\text{-}Htake}$/Nibio), were supplied by the JCRB Laboratory Animal Resource Bank at the National Institute of Biomedical Innovation. The experimental mouse protocols were approved by the Ethics Committee at the National Institute of Biomedical Innovation (assigned No. DS-23-35), and by the University of Toyama's Committee on Animal Experiments (assigned No. A2012eng-8) for animal welfare. For microarray analyses, cerebella were dissected after anesthesia of mice with isoflurane (WAKO Pure Chemicals, Osaka, JAPAN). The animals were maintained under standard light (08:00–20:00) and temperature conditions (23 °C, 50% humidity).

4.2. Reagents

Microsatellite markers were used to identify the chromosomal region responsible for the ataxic phenotype, (D6Mit86, 1.18 cM; D6Mit351, 22.94 cM; D6Mit384, 27.38 cM; D6Mit243, 32.2 cM 7;

D6Mit29, 37.75 cM; D6Mit102. 42.11 cM; D6Mit149, 48.93 cM; D6Mit200, 89.28 cM). To map the end points of the *Grid2* deletion, we used following primers: m*Grid2* intron 2H F 5'-GCT ACT TTG GTA CAA GTG GAC A and m*Grid2* intron 2H R 5'-GAC AAG TTG CTC TCT GTA TCT; m*Grid2* Intron 2I F 5'-CAT GCT CAC ATC AAA ATA CAT CAA and m*Grid2* Intron 2I R 5'-TGT AAT TGA GGAA AAT ACA TAA T. Other primers used in Figure 3D were prepared with reference to [31]. To identify the *Grid2* deletion in $Grid2^{Htake/Htake}$ mice, we used the following primers for PCR amplification: m*Grid2* Intron 2HIF 5'-TGG ATC CTT CTA CGT GCA AC, m*Grid2* Intron 8YF2 5'-GGA CCA CAC TGA GGT TCG AAA GA, and m*Grid2* Intron 8YR 5'-ATC TCT TGG CAT GCA TTA GAC. The mutant allele of $Grid2^{Htake}$ produces a PCR band corresponding to a product of approximately 600 bp, and that for the WT allele is approximately 400 bp.

GRID2 antibody was obtained from Santa Cruz Biotechnology (Santa Cruz, CA, USA). Antibodies for NMDAR1 and tubulin were obtained from Cell Signaling Technology (Boston, MA, USA). Memantine, AMPA, DNQX, MK-801, nitrazepam, donepezil, and ondansetron were purchased from WAKO Pure Chemicals; ifenprodil, Ro25-6981, DL-AP7, felbamate, and loperamide were obtained from Sigma-Aldrich (St. Louis, MO, USA).

4.3. mRNA Analyses

Total RNA was prepared from the cerebellar hemispheres of 12-week-old mice (male and female) using the EZ1-RNA purification kit (Qiagen, Venlo Park, The Netherlands). For microarray analyses, GeneChip Mouse Genome 430A (Affymetrix, Santa Clara, CA, USA) was used, and differences in transcript levels were calculated with Partek (Partek Inc., St. Louis, MO, USA). The original data files (CEL-files) were deposited in the Gene Expression Omnibus (GEO) repository and assigned the GEO accession numbers: GSM1334015, GSM1334016, and GSM1334017 for normal mice, and GSM1334018, GSM1334019, and GSM1334020 for mutant mice. PCR primers for real-time PCR were as follows: *mGrid2* F, 5'-AAC ACG CTA CAT GGA CTA CTC-3' and *mGrid2* R, 5'-GAA GCA CTG TGC CAG CAA TG-3'; m*Gapdh* F, 5'-ACT CAC GGC AAA TTC AAC GG-3' and m*Gapdh* R, 5'-GAC TCC ACG ACA TAC TGA GC-3'. To amplify the *Grid2* ORF, primers are mGrid2 F2 (5ATG): 5'-ATG GAA GTT TTC CCC TTG CTC TTG T and mGrid2 R (3Stop): 5'-TCA TAT GGA CGT GCC TCG GTC GGG GTC A were used.

4.4. Measurements of Walking Distance and the OKR

Male mice (12–14 weeks old) were placed in a rectangular box (25 cm × 40 cm), and their head position was tracked for 5 min using ANY-maze software (Brain Science Idea, Osaka, Japan). Each mouse was monitored three times, and the longest distance recorded was used in the data analysis.

The OKR was measured in adult mice using previously described methods [28], which are depicted in Supplementary Figure S1. Briefly, the mice were anesthetized with isoflurane (2%) and a stainless steel screw was glued to the skull. The mice were then habituated to the experimental conditions for 2 days before the measurement. Ten minutes before the measurement were made, mice were administered a saline (8 mL/kg) injection with or without memantine (10 mg/kg) intraperitoneally. The mouse was then mounted on a stereotaxic apparatus and exposed to continuous sinusoidal horizontal oscillations (17°, 0.25 Hz) of a cylindrical checkerboard-patterned screen (diameter, 65 cm; single

square, 1.8 × 1.8 cm; brightness, ~30 lx). Right eye movement was captured at 30 Hz with an infrared camera. For each image frame, we used a machine vision system to estimate the pupil azimuth from the location of the pupil center. The OKR was expressed on a time plot of the relative pupil azimuth for each round of screen oscillation, with the pupil azimuth at the beginning of backward eye movement set to 0°. An OKR gain was defined as the ratio of the maximal relative pupil azimuth change to that of the screen (17°).

4.5. Cell Culture and Electrophysiology

Granule cell-enriched cultures were prepared as previously described [61]. Briefly, 2-day-old (P2) mutant or WT mice were anesthetized by cooling and then sacrificed by decapitation. The cerebella were dissociated with trypsin, plated on poly-L-ornithine-coated plastic dishes (Becton Dickinson, Franklin Lakes, NJ, USA) at 1.25 million cells/mL, and maintained in low-serum, nutrient-supplemented Dulbecco's Modified Eagle Medium/F-12 (Life Technologies; 5% CO_2, 37 °C) for 12 days.

Ruptured-patch whole-cell recordings were performed on cultured granule cells. The pipette solution contained 134 mM potassium D-gluconic acid, 7.6 mM KCl, 9 mM KOH, 10 mM NaCl, 1.2 mM $MgCl_2$, 4 mM ATP magnesium salt, 10 mM HEPES, and 0.5 mM EGTA (pH 7.3). The culture dish was perfused at a rate of 1.4 mL/min with 145 mM NaCl, 5 mM KCl, 2 mM $CaCl_2$, 10 mM HEPES, 10 mM D-glucose, and 10 μM glycine (pH 7.4). Current signals were recorded using an EPC-8 amplifier (holding potential, −90 mV; cut-off frequency, 5 kHz; sampling rate, 20 kHz; HEKA, Lambrecht/Pfalz, Germany) controlled by Patchmaster software (version, 2.35; HEKA). The command potentials were corrected for a liquid junction potential between the pipette and bath solutions. Electronic capacitance cancellation and series resistance compensation were not used. The series resistance (33.2 ± 5.1 MΩ, n = 55) and membrane capacitance were estimated from the amplitude and time constant of the capacitive current evoked by a 10 mV voltage jump. The bath solution containing 20 μM NMDA or 10 μM memantine was locally applied to the cell through a theta tube under the control of gravity and electromagnetic valves (VM8, ALA Scientific Instruments, Farmingdale, NY, USA). The magnitude of an NMDA-induced current was quantified as the inward current charge over a 2 s NMDA application normalized to the membrane capacitance (charge density). The background charge was estimated from a 0.5 s pre-application period and subtracted from the charge density.

4.6. Statistical Analyses

Data from each group were characterized by the mean ± SD, unless otherwise stated. Data from biochemical assays were examined with one-way ANOVA followed by unpaired two-tailed *t*-tests to detect statistically significant differences. All the statistical examinations were performed using JMP software (versions 9.0.2 and 10.0.1, SAS Institute, Cary, NC, USA).

Acknowledgments

We thank Junko Morita for her technical assistance and Takayoshi Imazawa for their kind advice. We thank Sebnem Kesaf and Ryuichi Shigemoto for their advice on performing OKR measurements.

This study was supported by Grants-in-Aid for Scientific Research from the Ministry of Education, Culture, Sports, Science, and Technology, Japan (25670155, 23500384, 23500384); the grant from the Ministry of Health, Labor, and Welfare (2013–2017, 2014–2016); Scientific Research on Innovative Areas, a MEXT Grant-in-Aid Project 2012–2013; Strategic Research Foundation at Private Universities (2013–2017); the grant from the Human Science Foundation (2012–2013); and a grant from the Uehara Memorial Foundation.

Author Contributions

A.K., A.F., T.Y., Y.N., Y.H., T.S., Y.I., M.K., O.S., S.A, H.R., A.K., L.P.T, M.S., T.F., H.T. performed experiments. K.K., Y.N., H.K., K.M., T.N., J.M. T.T., H.T. analyzed data. T.T., H.T. wrote the manuscript.

Conflicts of Interest

No conflicts of interest, financial or otherwise, are declared by the author(s).

References

1. Sonkusare, S.K.; Kaul, C.L.; Ramarao, P. Dementia of Alzheimer's disease and other neurodegenerative disorders—Memantine, a new hope. *Pharmacol. Res.* **2005**, *51*, 1–17.
2. Lipton, S.A. Paradigm shift in neuroprotection by NMDA receptor blockade: Memantine and beyond. *Nat. Rev. Drug Discov.* **2006**, *5*, 160–170.
3. Szczurowska, E.; Mares, P. NMDA and AMPA receptors: Development and status epilepticus. *Physiol. Res.* **2013**, *62* (Suppl. 1), S21–S38.
4. Kupper, J.; Ascher, P.; Neyton, J. Probing the pore region of recombinant N-methyl-D-aspartate channels using external and internal magnesium block. *Proc. Natl. Acad. Sci. USA* **1996**, *93*, 8648–8653.
5. Wong, E.H.; Kemp, J.A.; Priestley, T.; Knight, A.R.; Woodruff, G.N.; Iversen, L.L. The anticonvulsant MK-801 is a potent N-methyl-D-aspartate antagonist. *Proc. Natl. Acad. Sci. USA* **1986**, *83*, 7104–7108.
6. Hansen, R.A.; Gartlehner, G.; Lohr, K.N.; Kaufer, D.I. Functional outcomes of drug treatment in Alzheimer's disease: A systematic review and meta-analysis. *Drugs Aging* **2007**, *24*, 155–167.
7. Uemura, T.; Lee, S.J.; Yasumura, M.; Takeuchi, T.; Yoshida, T.; Ra, M.; Taguchi, R.; Sakimura, K.; Mishina, M. Trans-synaptic interaction of GluRdelta2 and Neurexin through Cbln1 mediates synapse formation in the cerebellum. *Cell* **2010**, *141*, 1068–1079.
8. Matsuda, K.; Miura, E.; Miyazaki, T.; Kakegawa, W.; Emi, K.; Narumi, S.; Fukazawa, Y.; Ito-Ishida, A.; Kondo, T.; Shigemoto, R.; *et al.* Cbln1 is a ligand for an orphan glutamate receptor delta2, a bidirectional synapse organizer. *Science* **2010**, *328*, 363–368.
9. Kakegawa, W.; Miyoshi, Y.; Hamase, K.; Matsuda, S.; Matsuda, K.; Kohda, K.; Emi, K.; Motohashi, J.; Konno, R.; Zaitsu, K.; *et al.* D-Serine regulates cerebellar LTD and motor coordination through the delta2 glutamate receptor. *Nat. Neurosci.* **2011**, *14*, 603–611.

10. Jardon, B.; Bonaventure, N. N-Methyl-D-aspartate antagonists suppress the development of frog symmetric monocular optokynetic nystagmus observed after unilateral visual deprivation. *Brain Res. Dev. Brain Res.* **1992**, *67*, 67–73.
11. Godaux, E.; Cheron, G.; Mettens, P. Ketamine induces failure of the oculomotor neural integrator in the cat. *Neurosci. Lett.* **1990**, *116*, 162–167.
12. Mettens, P.; Cheron, G.; Godaux, E. NMDA receptors are involved in temporal integration in the oculomotor system of the cat. *Neuroreport* **1994**, *5*, 1333–1336.
13. Huang, Y.J.; Lin, C.H.; Lane, H.Y.; Tsai, G.E. NMDA Neurotransmission Dysfunction in Behavioral and Psychological Symptoms of Alzheimer's Disease. *Curr. Neuropharmacol.* **2012**, *10*, 272–285.
14. Puangthong, U.; Hsiung, G.Y. Critical appraisal of the long-term impact of memantine in treatment of moderate to severe Alzheimer's disease. *Neuropsychiatr. Dis. Treat.* **2009**, *5*, 553–561.
15. Utine, G.E.; Haliloglu, G.; Salanci, B.; Cetinkaya, A.; Kiper, P.O.; Alanay, Y.; Aktas, D.; Boduroglu, K.; Alikasifoglu, M. A Homozygous Deletion in GRID2 Causes a Human Phenotype With Cerebellar Ataxia and Atrophy. *J. Child Neurol.* **2013**, *28*, 926–932.
16. Maier, A.; Klopocki, E.; Horn, D.; Tzschach, A.; Holm, T.; Meyer, R.; Meyer, T. *De novo* partial deletion in GRID2 presenting with complicated spastic paraplegia. *Muscle Nerve* **2014**, *49*, 289–292.
17. Hills, L.B.; Masri, A.; Konno, K.; Kakegawa, W.; Lam, A.T.; Lim-Melia, E.; Chandy, N.; Hill, R.S.; Partlow, J.N.; Al-Saffar, M.; *et al.* Deletions in GRID2 lead to a recessive syndrome of cerebellar ataxia and tonic upgaze in humans. *Neurology* **2013**, *81*, 1378–1386.
18. Van Schil, K.; Meire, F.; Karlstetter, M.; Bauwens, M.; Verdin, H.; Coppieters, F.; Scheiffert, E.; van Nechel, C.; Langmann, T.; Deconinck, N.; *et al.* Early-onset autosomal recessive cerebellar ataxia associated with retinal dystrophy: New human hotfoot phenotype caused by homozygous GRID2 deletion. *Genet. Med.* **2014**, doi:10.1038/gim.2014.95.
19. Uebi, T.; Itoh, Y.; Hatano, O.; Kumagai, A.; Sanosaka, M.; Sasaki, T.; Sasagawa, S.; Doi, J.; Tatsumi, K.; Mitamura, K.; *et al.* Involvement of SIK3 in glucose and lipid homeostasis in mice. *PLOS ONE* **2012**, *7*, e37803.
20. Hemmings, H.C., Jr.; Yan, W.; Westphalen, R.I.; Ryan, T.A. The general anesthetic isoflurane depresses synaptic vesicle exocytosis. *Mol. Pharmacol.* **2005**, *67*, 1591–1599.
21. Rammes, G.; Danysz, W.; Parsons, C.G. Pharmacodynamics of memantine: An update. *Curr. Neuropharmacol.* **2008**, *6*, 55–78.
22. Seeman, P.; Caruso, C.; Lasaga, M. Memantine agonist action at dopamine D2High receptors. *Synapse* **2008**, *62*, 149–153.
23. Lee, J.W.; Park, H.J.; Choi, J.; Park, S.J.; Kang, H.; Kim, E.G. Comparison of ramosetron's and ondansetron's preventive anti-emetic effects in highly susceptible patients undergoing abdominal hysterectomy. *Korean J. Anesthesiol.* **2011**, *61*, 488–492.
24. Khojasteh, A.; Sartiano, G.; Tapazoglou, E.; Lester, E.; Gandara, D.; Bernard, S.; Finn, A. Ondansetron for the prevention of emesis induced by high-dose cisplatin. A multi-center dose-response study. *Cancer* **1990**, *66*, 1101–1105.
25. Jayadev, S.; Bird, T.D. Hereditary ataxias: Overview. *Genet. Med.* **2013**, *15*, 673–683.

26. Requena, T.; Espinosa-Sanchez, J.M.; Lopez-Escamez, J.A. Genetics of dizziness: Cerebellar and vestibular disorders. *Curr. Opin. Neurol.* **2014**, *27*, 98–104.
27. Rosini, F.; Federighi, P.; Pretegiani, E.; Piu, P.; Leigh, R.J.; Serra, A.; Federico, A.; Rufa, A. Ocular-motor profile and effects of memantine in a familial form of adult cerebellar ataxia with slow saccades and square wave saccadic intrusions. *PLOS ONE* **2013**, *8*, e69522.
28. Shirai, Y.; Asano, K.; Takegoshi, Y.; Uchiyama, S.; Nonobe, Y.; Tabata, T. A simple machine vision-driven system for measuring optokinetic reflex in small animals. *J. Physiol. Sci.* **2013**, *63*, 395–399.
29. Shutoh, F.; Ohki, M.; Kitazawa, H.; Itohara, S.; Nagao, S. Memory trace of motor learning shifts transsynaptically from cerebellar cortex to nuclei for consolidation. *Neuroscience* **2006**, *139*, 767–777.
30. Zuo, J.; de Jager, P.L.; Takahashi, K.A.; Jiang, W.; Linden, D.J.; Heintz, N. Neurodegeneration in Lurcher mice caused by mutation in delta2 glutamate receptor gene. *Nature* **1997**, *388*, 769–773.
31. Wang, Y.; Matsuda, S.; Drews, V.; Torashima, T.; Meisler, M.H.; Yuzaki, M. A hot spot for hotfoot mutations in the gene encoding the delta2 glutamate receptor. *Eur. J. Neurosci.* **2003**, *17*, 1581–1590.
32. Cull-Candy, S.G.; Wyllie, D.J. Glutamate-receptor channels in mammalian glial cells. *Ann. N. Y. Acad. Sci.* **1991**, *633*, 458–474.
33. Kato, A.S.; Knierman, M.D.; Siuda, E.R.; Isaac, J.T.; Nisenbaum, E.S.; Bredt, D.S. Glutamate receptor delta2 associates with metabotropic glutamate receptor 1 (mGluR1), protein kinase Cgamma, and canonical transient receptor potential 3 and regulates mGluR1-mediated synaptic transmission in cerebellar Purkinje neurons. *J. Neurosci.* **2012**, *32*, 15296–15308.
34. Hirai, H.; Launey, T.; Mikawa, S.; Torashima, T.; Yanagihara, D.; Kasaura, T.; Miyamoto, A.; Yuzaki, M. New role of delta2-glutamate receptors in AMPA receptor trafficking and cerebellar function. *Nat. Neurosci.* **2003**, *6*, 869–876.
35. Yamasaki, M.; Miyazaki, T.; Azechi, H.; Abe, M.; Natsume, R.; Hagiwara, T.; Aiba, A.; Mishina, M.; Sakimura, K.; Watanabe, M. Glutamate receptor delta2 is essential for input pathway-dependent regulation of synaptic AMPAR contents in cerebellar Purkinje cells. *J. Neurosci.* **2011**, *31*, 3362–3374.
36. Honore, T.; Davies, S.N.; Drejer, J.; Fletcher, E.J.; Jacobsen, P.; Lodge, D.; Nielsen, F.E. Quinoxalinediones: Potent competitive non-NMDA glutamate receptor antagonists. *Science* **1988**, *241*, 701–703.
37. Kakegawa, W.; Miyazaki, T.; Kohda, K.; Matsuda, K.; Emi, K.; Motohashi, J.; Watanabe, M.; Yuzaki, M. The N-terminal domain of GluD2 (GluRdelta2) recruits presynaptic terminals and regulates synaptogenesis in the cerebellum *in vivo*. *J. Neurosci.* **2009**, *29*, 5738–5748.
38. Rabacchi, S.; Bailly, Y.; Delhaye-Bouchaud, N.; Mariani, J. Involvement of the N-methyl D-aspartate (NMDA) receptor in synapse elimination during cerebellar development. *Science* **1992**, *256*, 1823–1825.
39. Garthwaite, J.; Brodbelt, A.R. Synaptic activation of N-methyl-D-aspartate and non-N-methyl-D-aspartate receptors in the mossy fibre pathway in adult and immature rat cerebellar slices. *Neuroscience* **1989**, *29*, 401–412.

40. Yuzaki, M.; Forrest, D.; Verselis, L.M.; Sun, S.C.; Curran, T.; Connor, J.A. Functional NMDA receptors are transiently active and support the survival of Purkinje cells in culture. *J. Neurosci.* **1996**, *16*, 4651–4661.
41. Balazs, R.; Jorgensen, O.S.; Hack, N. N-Methyl-D-aspartate promotes the survival of cerebellar granule cells in culture. *Neuroscience* **1988**, *27*, 437–451.
42. Ortega, F.; Perez-Sen, R.; Morente, V.; Delicado, E.G.; Miras-Portugal, M.T. P2X7, NMDA and BDNF receptors converge on GSK3 phosphorylation and cooperate to promote survival in cerebellar granule neurons. *Cell. Mol. Life Sci.* **2010**, *67*, 1723–1733.
43. Kadotani, H.; Hirano, T.; Masugi, M.; Nakamura, K.; Nakao, K.; Katsuki, M.; Nakanishi, S. Motor discoordination results from combined gene disruption of the NMDA receptor NR2A and NR2C subunits, but not from single disruption of the NR2A or NR2C subunit. *J. Neurosci.* **1996**, *16*, 7859–7867.
44. Marmolino, D.; Manto, M. Past, present and future therapeutics for cerebellar ataxias. *Curr. Neuropharmacol.* **2010**, *8*, 41–61.
45. Bormann, J. Memantine is a potent blocker of N-methyl-D-aspartate (NMDA) receptor channels. *Eur. J. Pharmacol.* **1989**, *166*, 591–592.
46. Strupp, M.; Brandt, T. Current treatment of vestibular, ocular motor disorders and nystagmus. *Ther. Adv. Neurol. Disord.* **2009**, *2*, 223–239.
47. Yoshida, T.; Katoh, A.; Ohtsuki, G.; Mishina, M.; Hirano, T. Oscillating Purkinje neuron activity causing involuntary eye movement in a mutant mouse deficient in the glutamate receptor delta2 subunit. *J. Neurosci.* **2004**, *24*, 2440–2448.
48. Faulstich, M.; van Alphen, A.M.; Luo, C.; du Lac, S.; De Zeeuw, C.I. Oculomotor plasticity during vestibular compensation does not depend on cerebellar LTD. *J. Neurophysiol.* **2006**, *96*, 1187–1195.
49. Gordon, J.W.; Uehlinger, J.; Dayani, N.; Talansky, B.E.; Gordon, M.; Rudomen, G.S.; Neumann, P.E. Analysis of the hotfoot (ho) locus by creation of an insertional mutation in a transgenic mouse. *Dev. Biol.* **1990**, *137*, 349–358.
50. Kashiwabuchi, N.; Ikeda, K.; Araki, K.; Hirano, T.; Shibuki, K.; Takayama, C.; Inoue, Y.; Kutsuwada, T.; Yagi, T.; Kang, Y.; *et al.* Impairment of motor coordination, Purkinje cell synapse formation, and cerebellar long-term depression in GluR delta 2 mutant mice. *Cell* **1995**, *81*, 245–252.
51. Wilson, D.B. Brain abnormalities in the lurcher (Lc) mutant mouse. *Experientia* **1975**, *31*, 220–221.
52. Nishiyama, J.; Matsuda, K.; Kakegawa, W.; Yamada, N.; Motohashi, J.; Mizushima, N.; Yuzaki, M. Reevaluation of neurodegeneration in lurcher mice: Constitutive ion fluxes cause cell death with, not by, autophagy. *J. Neurosci.* **2010**, *30*, 2177–2187.
53. Cendelin, J.; Tuma, J.; Korelusova, I.; Vozeh, F. The effect of genetic background on behavioral manifestation of Grid2(Lc) mutation. *Behav. Brain Res.* **2014**, *271*, 218–227.
54. Schwartz, E.J.; Rothman, J.S.; Dugue, G.P.; Diana, M.; Rousseau, C.; Silver, R.A.; Dieudonne, S. NMDA receptors with incomplete Mg(2)(+) block enable low-frequency transmission through the cerebellar cortex. *J. Neurosci.* **2012**, *32*, 6878–6893.
55. Hepp, R.; Hay, Y.A.; Aguado, C.; Lujan, R.; Dauphinot, L.; Potier, M.C.; Nomura, S.; Poirel, O.; El Mestikawy, S.; Lambolez, B.; *et al.* Glutamate receptors of the delta family are widely expressed in the adult brain. *Brain Struct. Funct.* **2014**, doi:10.1007/s00429-014-0827-4.

56. Glitsch, M.D. Calcium influx through N-methyl-D-aspartate receptors triggers GABA release at interneuron-Purkinje cell synapse in rat cerebellum. *Neuroscience* **2008**, *151*, 403–409.
57. Liu, S.J. Biphasic modulation of GABA release from stellate cells by glutamatergic receptor subtypes. *J. Neurophysiol.* **2007**, *98*, 550–556.
58. Duguid, I.C.; Smart, T.G. Retrograde activation of presynaptic NMDA receptors enhances GABA release at cerebellar interneuron-Purkinje cell synapses. *Nat. Neurosci.* **2004**, *7*, 525–533.
59. Hirano, T.; Watanabe, D.; Kawaguchi, S.Y.; Pastan, I.; Nakanishi, S. Roles of inhibitory interneurons in the cerebellar cortex. *Ann. N. Y. Acad. Sci.* **2002**, *978*, 405–412.
60. Whittingham, D.G. Fertilization of mouse eggs *in vitro*. *Nature* **1968**, *220*, 592–593.
61. Tabata, T.; Sawada, S.; Araki, K.; Bono, Y.; Furuya, S.; Kano, M. A reliable method for culture of dissociated mouse cerebellar cells enriched for Purkinje neurons. *J. Neurosci. Methods* **2000**, *104*, 45–53.

Leukemia Research xxx (2014) xxx–xxx

Contents lists available at ScienceDirect

Leukemia Research

journal homepage: www.elsevier.com/locate/leukres

Commentary

Cell line cross-contamination: WSU-CLL is a known derivative of REH and is unsuitable as a model for chronic lymphocytic leukaemia

A recent article by Zhang et al. [1] explored the mechanism of action of arsenic trioxide in induction of apoptosis. The study used a single cell line, WSU-CLL, as a model for B-cell chronic lymphocytic leukaemia (B-CLL). As the authors noted, arsenic trioxide is a possible therapeutic agent for a number of malignancies, including B-CLL. Their results might therefore be clinically relevant to patients with this disorder.

The conclusions reached by Zhang et al. [1] seem straightforward at first glance. But a closer look at the scientific literature reveals an obvious problem. The WSU-CLL cell line is known to be a false or misidentified cell line [2,3]. DNA profiling and cytogenetic analysis performed by the Deutsche Sammlung von Mikroorganismen und Zellkulturen (DSMZ) [2] demonstrated that WSU-CLL is actually REH, a cell line derived from B-cell precursor acute lymphoblastic leukaemia (BCP-ALL). These cells carry the ETV6-AML1 fusion rearrangement recurrently reported in BCP-ALL, but not in B-CLL [4]. The stocks of WSU-CLL that were tested by DSMZ came directly from the originators of the cell line; no other authentic stocks have been found [3]. It is likely that WSU-CLL was cross-contaminated during establishment, resulting in overgrowth of WSU-CLL and replacement with REH cells. The end result is a false cell line that no longer corresponds to B-CLL.

The finding that WSU-CLL is a false cell line does not invalidate the data presented by Zhang et al. [1]. It is reasonable to conclude that arsenic trioxide induces apoptosis in WSU-CLL cells, through down-regulation of survivin, in a p53-dependent manner. However, not all of the authors' conclusions can be substantiated. The identity of the cell line becomes critically important when deciding if arsenic trioxide should be used as a therapeutic agent for patients with chronic lymphocytic leukaemia.

A closer analysis of the literature shows why authors may incorrectly assume that WSU-CLL is a valid model for chronic lymphocytic leukaemia (Table 1 and Supplementary Data). We examined 27 references that referred to WSU-CLL in their abstracts or methods, dating from the initial characterisation of the cell line in 1996 [5]. Of these 27 references, three referred to WSU-CLL using its correct tissue attribution (BCP-ALL). The remaining 24 references reported WSU-CLL as a cell line arising from B-CLL. These 24 references were published in 15 different journals.

The potential impact of this reporting became more evident when we looked at the number of citations per reference. The three references that referred to WSU-CLL as an acute lymphoblastic leukaemia cell line were cited 215 times (Table 1 and Supplementary Data). In contrast, the 24 references that reported WSU-CLL as a chronic lymphocytic leukaemia cell line were cited 1159 times.

It should be made clear that the 24 references using WSU-CLL as a model for B-CLL relied on the information available to them at the time of publication. The majority of references using WSU-CLL were published before 2002, when cross-contamination of the cell line was first discovered [2]. However, authors reading those papers today could easily conclude that WSU-CLL is an appropriate model for chronic lymphocytic leukaemia.

Cell lines are widely used and are essential models for biomedical research. In the same issue as Zhang's publication, another 20 cell lines were used as models for leukaemia and lymphoma (Supplementary Data). It is difficult to know if other cell lines have been incorrectly reported, without looking specifically at each instance as part of the manuscript submission process. We therefore urge Leukaemia Research, and other journals that publish cell line data, to respond to false cell lines by adopting new requirements for authors.

We urge all laboratories to check the authenticity of their cell lines before starting work. Checking for authenticity should involve a search of the scientific literature, which in this case, would clearly indicate that the WSU-CLL cell line is cross-contaminated [2]. It may not always be easy to find a publication demonstrating that a cell line is misidentified. To assist the research community, the International Cell Line Authentication Committee (ICLAC) curates a database of known cross-contaminated or otherwise misidentified cell lines [6]. The database, which continues to be updated, is available at www.iclac.org.

It is also essential for authors to check their own cell line stocks by performing authentication testing. The original report that WSU-CLL is cross-contaminated relied on short tandem repeat (STR) profiling and cytogenetic analysis [2]. STR profiling has now been adopted by many laboratories and an international standard has been published, containing a consensus approach to testing of human cell lines [7]. Shared databases of human cell line STR profiles are available online for comparison to cell line stocks worldwide [8].

Adopting minimum reporting requirements for cell lines would be a simple and straightforward way to address the problem. We urge authors to report in their manuscripts whether authentication testing has been performed for the cell line(s) used, and which method(s) were used for authentication. Authentication testing of

http://dx.doi.org/10.1016/j.leukres.2014.05.003
0145-2126/

Table 1
Reporting of WSU-CLL in published journal articles.

	Reported as CLL (incorrect)	Reported as ALL (correct)
Published articles referring to WSU-CLL	24	3
Journals in which these articles were published	15	2
Citations of published articles referring to WSU-CLL	1159	215

The table summarises the ways in which WSU-CLL has been reported and estimates the impact of this reporting in published journal articles. Published articles that refer to WSU-CLL were collated by performing a search for "WSU-CLL" using PubMed and Google. For each article, we documented the journal in which that article was published, and the number of citations using Web of Science (Thomson Reuters). Each article was then examined for its description of WSU-CLL. All articles referred to WSU-CLL as arising from a specific tissue, or used the cell line as a control for a specific tissue – either chronic lymphocytic leukaemia (CLL) or acute lymphoblastic leukaemia (ALL).

human cells should include STR profiling, allowing comparison to donor tissue or other commonly used cell lines. Species determination, at a minimum, should be performed for non-human cell lines.

We also encourage a standardised framework for reporting cell line data, with inclusion of minimum criteria to encourage transparency and reproducibility. Authors should include the full name of any cell line used; its source and catalogue number; the range of passage numbers used; and whether the cell line has been tested for contamination, with the method used and the results. Essential quality control evaluation should include both mycoplasma testing and authentication testing, regardless of the cell line application.

In the absence of any institutional mechanism for enforcing their withdrawal, false cell lines such as WSU-CLL remain prevalent within the scientific literature. Their use has led to the scientific record becoming increasingly inaccurate and unreliable. We invite all who handle cell lines, and all who publish or fund such work, to address the problem by working towards a standardised reporting framework with minimal criteria for cell line data.

Conflicts of interest statement

One of the contributors is employed by LabCorp, which offers commercial cell line authentication services.

Role of the funding source

ICLAC is a voluntary committee. Costs associated with website development and maintenance are reimbursed through funding arrangements as declared on the ICLAC website. This funding had no involvement in the preparation of this manuscript or the decision to submit for publication.

Acknowledgements

Contributors: HGD and ACD initiated the comment, which ACD drafted on behalf of the International Cell Line Authentication Committee (ICLAC). ACD performed the data analysis as set out in the Supplementary Data. All authors contributed as ICLAC members to the conception of the comment, its revision, and approval of the final version.

Appendix A. Supplementary data

Supplementary material related to this article can be found, in the online version, at http://dx.doi.org/10.1016/j.leukres.2014.05.003.

References

[1] Zhang XH, Feng R, Lv M, Jiang Q, Zhu HH, Qing YZ, et al. Arsenic trioxide induces apoptosis in B-cell chronic lymphocytic leukemic cells through down-regulation of survivin via the p53-dependent signaling pathway. Leuk Res 2013;37:1719–25.
[2] Drexler HG, Quentmeier H, Dirks WG, Uphoff CC, MacLeod RA. DNA profiling and cytogenetic analysis of cell line WSU-CLL reveal cross-contamination with cell line REH (pre B-ALL). Leukemia 2002;16:1868–70.
[3] Drexler HG, Dirks WG, Matsuo Y, MacLeod RA. False leukemia–lymphoma cell lines: an update on over 500 cell lines. Leukemia 2003;17:416–26.
[4] Uphoff CC, MacLeod RA, Denkmann SA, Golub TR, Borkhardt A, Janssen JW, et al. Occurrence of TEL-AML1 fusion resulting from (12;21) translocation in human early B-lineage leukemia cell lines. Leukemia 1997;11:441–7.
[5] Mohammad RM, Mohamed AN, Hamdan MY, Vo T, Chen B, Kanato K, et al. Establishment of a human B-CLL xenograft model: utility as a preclinical therapeutic model. Leukemia 1996;10:130–7.
[6] Capes-Davis A, Theodosopoulos G, Atkin I, Drexler HG, Kohara A, Macleod RA, et al. Check your cultures! A list of cross-contaminated or misidentified cell lines. Int J Cancer 2010;127:1–8.
[7] ANSI/ATCC ASN-0002-2011. Authentication of Human Cell Lines: Standardization of STR Profiling. ANSI eStandards Store; 2012. http://webstore.ansi.org/
[8] Dirks WG, MacLeod RA, Nakamura Y, Kohara A, Reid Y, Milch H, et al. Cell line cross-contamination initiative: an interactive reference database of STR profiles covering common cancer cell lines. Int J Cancer 2010;126:303–4.

the International Cell Line Authentication Committee (ICLAC)
Amanda Capes-Davis[a,*]
Christine Alston-Roberts[b]
Tanya Barrett[c]
Edward C. Burnett[d]
Jim R. Cooper[d]
Wilhelm G. Dirks[e]
R. Ian Freshney[f]
James R. Fuller[g]
Lyn Healy[h]
Liz Kerrigan[b]
Douglas A. Kniss[i]
Arihiro Kohara[j]
Christopher Korch[k]
Roderick A.F. MacLeod[e]
John R.W. Masters[l]
Yukio Nakamura[m]
Roland M. Nardone[n]
Raymond W. Nims[o]
Yvonne A. Reid[b]
Douglas R. Storts[p]
Hans G. Drexler[e]
[a] *CellBank Australia – Children's Medical Research Institute, Westmead, New South Wales, Australia*
[b] *American Type Culture Collection (ATCC), Manassas, VA, United States*
[c] *National Center for Biotechnology Information (NCBI), National Library of Medicine (NLM), National Institutes of Health (NIH), Bethesda MD, United States*
[d] *Culture Collections Public Health England, Porton Down, United Kingdom*
[e] *Leibniz-Institut Deutsche Sammlung von Mikroorganismen und Zellkulturen (DSMZ), Braunschweig, Germany*
[f] *Institute of Cancer Sciences, University of Glasgow, Glasgow, United Kingdom*
[g] *DNA Identification Testing Division, Laboratory Corporation of America, Burlington, NC, United States*

Please cite this article in press as: Cell line cross-contamination: WSU-CLL is a known derivative of REH and is unsuitable as a model for chronic lymphocytic leukaemia. Leuk Res (2014), http://dx.doi.org/10.1016/j.leukres.2014.05.003

[h] UK Stem Cell Bank, National Institute for Biological Standards and Control, Potters Bar, United Kingdom
[i] Departments of Obstetrics & Gynecology and Biomedical Engineering, The Wexner Medical Center at Ohio State University, Columbus, OH, United States
[j] Japanese Collection of Research Bioresources (JCRB), National Institute of Biomedical Innovation, Osaka, Japan
[k] DNA Sequencing and Analysis Core, University of Colorado School of Medicine, Aurora, CO, United States
[l] The Prostate Cancer Research Centre, University College London, London, United Kingdom
[m] RIKEN BioResource Center, Cell Engineering Division, Tsukuba, Japan
[n] Catholic University of America, Washington, DC, United States
[o] RMC Pharmaceutical Solutions, Longmont, CO, United States
[p] Promega Corporation, Madison, WI, United States

29 April 2014

4 May 2014
Available online xxx

Please cite this article in press as: Cell line cross-contamination: WSU-CLL is a known derivative of REH and is unsuitable as a model for chronic lymphocytic leukaemia. Leuk Res (2014), http://dx.doi.org/10.1016/j.leukres.2014.05.003

DNA Research **21**, 673–683, (2014) doi:10.1093/dnares/dsu029
Advance Access publication on 28 September 2014

The Genome Landscape of the African Green Monkey Kidney-Derived Vero Cell Line

Naoki Osada[1,†], Arihiro Kohara[2,†], Toshiyuki Yamaji[3], Noriko Hirayama[2], Fumio Kasai[2], Tsuyoshi Sekizuka[4], Makoto Kuroda[4], and Kentaro Hanada[3,*]

Division of Evolutionary Genetics, Department of Population Genetics, National Institute of Genetics, Mishima, Shizuoka 411-8540, Japan[1]; Laboratory of Cell Cultures, National Institute of Biomedical Innovation, Ibaraki, Osaka 567-0085, Japan[2]; Department of Biochemistry and Cell Biology, National Institute of Infectious Diseases, Tokyo 162-8640, Japan[3] and Pathogen Genomics Center, National Institute of Infectious Diseases, Tokyo 162-8640, Japan[4]

*To whom correspondence should be addressed. Tel. +81 3-5285-1158. Fax. +81 3-5285-1157.
Email: hanak@nih.go.jp

Edited by Prof. Masahira Hattori
(Received 2 July 2014; accepted 1 September 2014)

Abstract

Continuous cell lines that originate from mammalian tissues serve as not only invaluable tools for life sciences, but also important animal cell substrates for the production of various types of biological pharmaceuticals. Vero cells are susceptible to various types of microbes and toxins and have widely contributed to not only microbiology, but also the production of vaccines for human use. We here showed the genome landscape of a Vero cell line, in which 25,877 putative protein-coding genes were identified in the 2.97-Gb genome sequence. A homozygous ~9-Mb deletion on chromosome 12 caused the loss of the type I interferon gene cluster and cyclin-dependent kinase inhibitor genes in Vero cells. In addition, an ~59-Mb loss of heterozygosity around this deleted region suggested that the homozygosity of the deletion was established by a large-scale conversion. Moreover, a genomic analysis of Vero cells revealed a female *Chlorocebus sabaeus* origin and proviral variations of the endogenous simian type D retrovirus. These results revealed the genomic basis for the non-tumourigenic permanent Vero cell lineage susceptible to various pathogens and will be useful for generating new sub-lines and developing new tools in the quality control of Vero cells.

Key words: Vero cell; whole genome; infectious diseases; vaccine; animal cell substrate

1. Introduction

Continuous cell lines that originate from mammalian tissues serve as not only invaluable tools for life sciences, but also important animal cell substrates for the production of various types of biological pharmaceuticals. One lineage of the most frequently utilized mammalian cell lines for these purposes is the Vero cell lineage, which was established from the kidney tissue of an African green monkey (AGM). The primary culture of this tissue was started on 27 March 1962 in Chiba University in Japan, several continuous cell sub-lines were obtained after passages for several months, and a sub-line was then chosen as the standard Vero cell line.[1,2]

Vero cells were found to be highly susceptible to various types of viruses including simian polyoma virus SV-40,[1,2] measles virus,[3] rubella virus,[4,5] arboviruses,[6,7] and adenoviruses[7] soon after their establishment, and were later found to be also susceptible to bacterial toxins including the diphtheria toxin,[8] heat-labile enterotoxins,[9] and Shiga-like toxins (or 'Vero' toxins).[10,11] After their global distribution,[12,13] the application range of Vero cells extended from virology in academic laboratories to diagnostic practices in hospitals and bacterial toxin assays. Vero cells have pseudo-

† These authors contributed equally to this study and, thus, are the co-first authors.

diploid karyotypes[14] and are non-tumourigenic when a cell passage was not prolonged.[15,16] Therefore, the Vero cell lineage has been successfully utilized as a cell substrate for human vaccines.[17,18] Vero cells are still the first choice cell model for various types of life-threating emerging pathogens such as H5N1 influenza virus,[19] Ebola haemorrhagic fever virus,[20] and middle east respiratory syndrome (MERS) coronavirus.[21] Animal substrates for vaccine manufacturing are desired to be shifted from animals and eggs to assured continuous cell lines, because animal materials have several concerns related to quality control, stable supply, and animal ethics.[17–19] In addition, antigenic drift affecting the vaccination efficacy to humans, which often occurs during the proliferation of influenza viruses in hen eggs,[22] might be improved by shifting to vaccine strain-susceptible human or non-human primate culture cells.

Therefore, the Vero cell lineage should be fully characterized using modern technologies to prepare threats of infectious diseases. The whole-genome sequences of continuous cell lines provide invaluable basic information for various purposes. The genome sequence of a cell line is a comprehensive basis for many genetic characteristics of the cell line, it is closely relevant to other omics approaches such as transcriptomics and proteomics on the cell line, and also facilitates targeted genome editing of the cell line.[23–25] However, the whole genome of Vero cells has not yet been determined. We here provided a draft sequence of the whole genome of the Vero cell lineage after massively parallel sequencing of the genome DNA and also karyological and RNA-seq analyses. The genome landscape gave a mechanical insight into events that had occurred during the establishment of the permanent cell line susceptible to various types of microbes. In addition, we presented a proof of concept for the genomic-based quality control of cell lines.

2. Materials and methods

2.1. *Karyological analysis*

Metaphase chromosomes from Vero cells and AGM peripheral blood mononuclear cells (PBMC) were analysed by conventional Giemsa-banding (G-banding)[26] and multi-colour fluorescence *in situ* hybridization (M-FISH) with 24 differentially labelled human chromosome-specific painting probes (24xCyte kit MetaSystems, Altlussheim, Germany). For detailed information, see Supplementary data.

2.2. *Genome DNA preparation and de novo assembly*

Genome DNA was prepared from Vero cells (with passage number 115) and PBMC using the Qiagen Blood & Cell Culture DNA kit (Qiagen GmbH, Hilden, Germany). Libraries constructed for paired ends and mate pairs were sequenced with HiSeq2,000 (Illumina Inc., San Diego, California). After quality filtering, sequences were assembled into scaffolds using SGA and SSPACE software[27,28] (see Supplementary data for detailed assembly procedure). Protein-coding genes were predicted by the AUGUSTUS program with reference to the human genome as a model[29] and also with RNA-seq reads to assist in the predictions.

2.3. *Mapping to the rhesus macaque and AGM reference genome*

Reads were mapped on the draft genome of the rhesus macaque (*Macaca mulatta*: rheMac2) and AGM (*Chlorocebus sabaeus* 1.0: GCA_000409795.1) using the BWA-MEM algorithm with default parameter settings.[30] After mapping, potential polymerase chain reaction (PCR) duplicates, which were mapped to the same positions of the reference genome, were removed using Picard software (http://picard.sourceforge.net). The average genome coverage of paired-end sequences after removing the PCR duplicates was 54-fold for the AGM reference. Single-nucleotide variants (SNVs) were called following the Best Practice pipeline of the Genome Analysis Toolkit (GATK) software package, which includes base quality score recalibration, insertion/deletion (indel) realignment, and discovering and filtering SNVs and indels.[31]

2.4. *Detection of genomic rearrangements in the Vero JCRB0111 cell line*

Copy number variants were detected using the Control-FREEC software[32] with a 100-kb window size and 20-kb step size. Sites with map quality scores <40 were not used in the analysis. Structural variants were identified using the integrated structural variant prediction method DELLY. Junction sequences with $\geq 85\%$ identity to the other part of the reference genome and split-read coverage >100 were also filtered out.

To reduce rare and false-positive variant calls, we further applied the following conservative criteria. To detect deletions and inversions, we counted reads spanning non-rearranged sequence regions with at least 7 bp overlapping to each sequence proximal and distal to the boundaries. The number of these canonical reads should be proportional to the number of non-rearranged cells. The number of canonical reads was calculated for each non-rearranged region and divided by 2, because one rearrangement had two non-rearranged regions. We selected the regions at which rearranged reads (split reads) consisted of at least 70% of total reads mapped on boundary regions (sum of canonical and split reads). We also filtered out the regions that had <20 paired-end supports. For additional information, see Supplementary data.

Loss-of-heterozygosity (LOH) regions were identified using 1-Mb-size windows with average heterozygosity <0.0005 and the ratio of homozygous to heterozygous SNVs smaller than 0.2. The cut-off criteria were determined using the distribution of these values in a whole genome (Supplementary Fig. S3). The windows were progressively merged into larger regions when average statistics in the region satisfied the criteria.

2.5. *Miscellaneous*

Procedures for cell culture, tumourigenicity test, RNA-seq, phylogenetic analysis, and genomic PCR are described in Supplementary data.

2.6. *Ethics*

All animal experimental procedures were approved by the National Institute of Biomedical Innovation Committee on Animal Resources as the Institutional Animal Care and Use Committee.

2.7. *Accession codes*

The short reads and assembled draft genome sequence have been deposited in the public database (accession number: DRA002256). The full-length simian endogenous retrovirus sequences obtained in Vero JCRB0111 cells have been deposited in DDBJ (accession number: AB935214).

3. Results

3.1. *Vero cell seed*

To obtain the reference genome sequence of the cell lineage, cell seeds with the least passage levels were desirable as material. We chose a cryopreserved cell lot registered at the Japanese Collection of Research Bioresources Cell Bank, which, to the best of our knowledge, is the oldest or nearly the oldest lot (with a passage level of 115 from the original primary culture started in March 1962) among the currently available stocks. Lot JCRB0111 (hereafter referred to as Vero JCRB0111) was expected to be a close relative to widely distributed Vero cell seeds such as ATCC CCL81 and WHO Vero 10–87.[1,2,12,13,33–35] The heteroplantation of Vero JCRB0111 cells in immunocompromised nude mice ($n = 10$) did not produce any discernible tumours, while that of human cervical carcinoma-derived HeLa cells produced tumours in nude mice at 100% efficacy. Thus, Vero JCRB0111 cells are non-tumourigenic, which is consistent with previous findings of Vero cells being non-tumourigenic when their passage number was limited.[15,16]

When choosing the Vero JCRB0111 cell seed in this study, we confirmed that there was no microbial contamination in the seed using conventional tests. In addition, DNA-seq short reads, which were obtained to resolve the draft sequence of the whole Vero cell genome, were employed to comprehensively detect microbe-relevant sequences with a megablast search. No discernible sign of microbe-relevant sequences (except for endogenous retroviral sequences as shown below) was detected in the cell genome sample, which confirmed the absence of microbial contamination in the Vero cell seed.

3.2. *Karyotyping*

The Vero JCRB0111 cell line had different karyotypes with chromosomes numbering between 52 and 62, and the modal chromosome number appeared to be 59 chromosomes in 79 of 100 metaphase cells (Fig. 1A). The same analysis on PBMC from normal female AGM showed 60 chromosomes (Supplementary Fig. S1A).[36] Because the G-banding karyotypes of Vero cells include several abnormal chromosomes (Fig. 1B), M-FISH was applied to identify chromosomal rearrangements. Human M-FISH probes hybridized efficiently to AGM chromosomes and showed 32 syntenic blocks in normal AGM karyotypes (Fig. 1C). This homology to humans was consistent with previous findings,[37] and implied that the human M-FISH signal pattern can be used as a normal AGM reference (Fig. 1C). G-banding and M-FISH analyses revealed that 18 of 37 Vero metaphases represented a main clone with 59 chromosomes. M-FISH identified 40 segments in the Vero metaphases (Fig. 1D), which indicated the occurrence of one fusion and seven translocations. The fusion occurring between chromosomes 7 and 24 led to a reduction in the chromosome number from 60 to 59. Duplications and deletions were also detected in 6 chromosomes (Fig. 1D), showing rearrangements involved in 14 chromosomes. However, major chromosomal rearrangements were not detected in the other 46 chromosomes by G-banding or M-FISH (Fig. 1B and D), which suggested that a haploid chromosome set was retained in its original form. In addition to these common features, additional abnormalities were detected in 11 of 37 cells (Supplementary Fig. S1C and D). Although the other eight karyotypes were found to have similar abnormalities, the Vero cell line appeared to include several subclones. The main clone accounted for less than half of the population (18 of 37 cells) and the Vero cell line had a high cytogenetic heterogeneity.

3.3. *De novo assembly of the Vero genome sequence*

Two paired-end and three different size mate-pair libraries were constructed from Vero cell DNA, and the libraries were sequenced by massively parallel sequencing. The insert size distribution and read length of the libraries are summarized in Supplementary Table S1. After quality filtering, we obtained a total of ~2.55 billion paired-end and 390 million mate-pair reads.

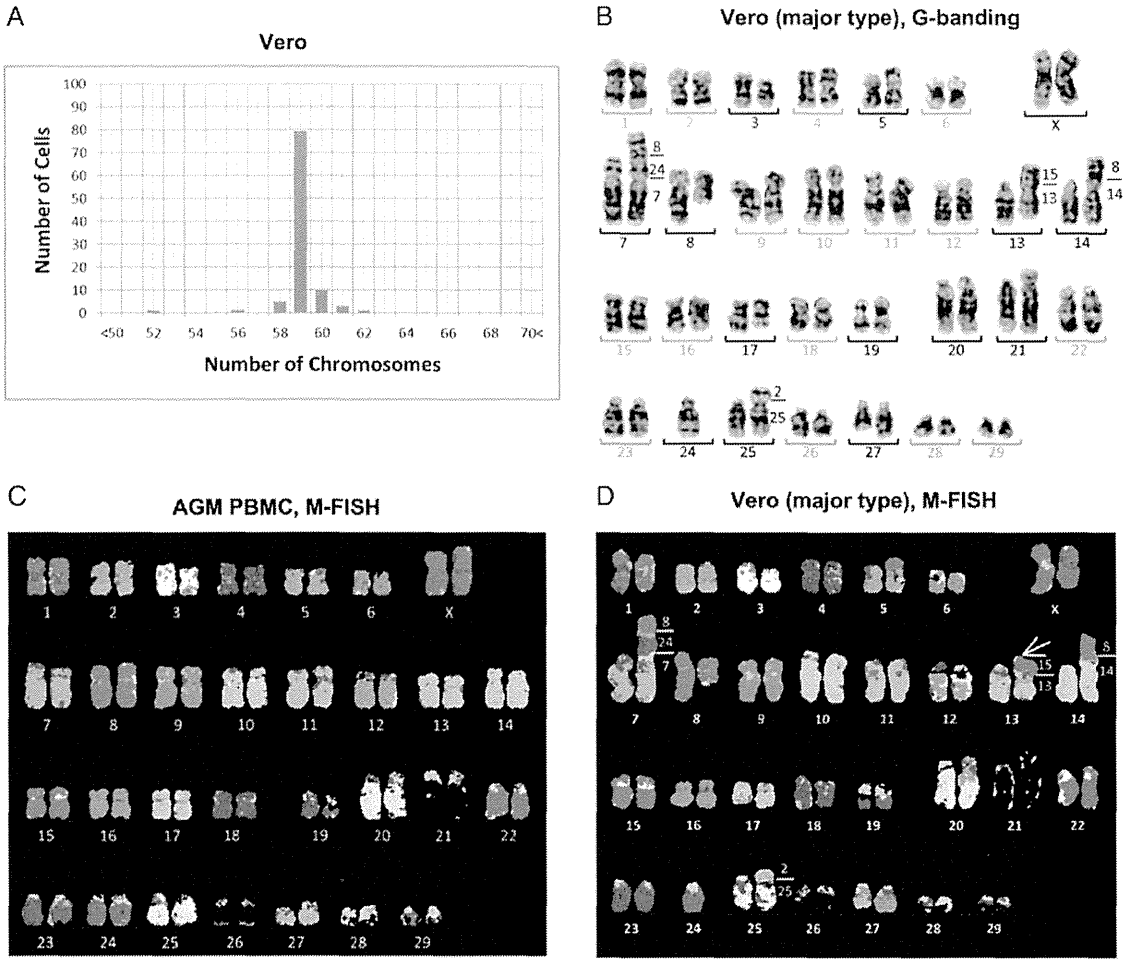

Figure 1. Karyotyping of the Vero JCRB0111 cell line. (A) Chromosome number in the Vero cell line based on 100 Giemsa-stained metaphases, which showed that the modal number was 59 chromosomes and differences in the chromosome number between 52 and 62 indicated heterogeneous karyotypes. (B) G-banded karyotype of Vero cells with 59 chromosomes consisted of 16 homologous pairs (blue numbers) and 13 abnormal chromosomes (black numbers). (C and D) M-FISH signal pattern using human probes on a normal AGM metaphase (C), and a main clone of the Vero cell line (D). Paints of human chromosomes 1–22 and X showed homologous regions in the AGF and the identity of 32 and 40 syntenic blocks in a normal female and Vero, respectively. The number on the right of aberrant chromosomes (D) shows correspondence to AGF chromosomes. The derivative chromosome der(13) (white arrow in D) showed an extra signal that corresponded to AGM chromosomes 15 and 22, both of which were painted by human chromosome 3. Although the addition in der(13) could not be distinguished using human M-FISH probes, the copy number analysis revealed a gain at chromosome 15q (Fig. 2B), which indicated that der(13) had additional material over chromosome 15.

The filtered sequences were used for *de novo* assembly of the Vero genome. Our final scaffolds consisted of 401,905 scaffolds, which were 2.97 Gb in total, and had the N50 of 508 kb and N90 of 48 kb. The AUGUSTUS program identified 25,877 putative protein-coding genes in the genome scaffolds, using RNA-seq data as a support.

3.4. *The female C. sabaeus origin of the Vero cell lineage*

The Vero cell lineage was originally reported to be established from the kidney of the AGM *Cercopithecus aethiops*.[1,2] However, the species classification of AGMs is a still debated issue and has been revised several times.[38,39] In current nomenclature, *Cercopithecus aethiops* is further classified into four different species of *Chlorocebus*. To clarify the species origin of the Vero cell lineage, we compared our reads with four previously reported complete mitochondrial sequences of *Chlorocebus* species: *Chlorocebus aethiops*, *Chlorocebus tantalus*, *C. sabaeus*, and *Chlorocebus pygerythrus*.[40] The mutation rate in the mitochondrial genomes of Old World monkeys is known to be markedly higher than that in nuclear genomes[41]; therefore, the mitochondrial sequences of these four species had sufficiently diverged to cause mapping bias of short reads. We mapped the paired-end reads to all four *Chlorocebus* mitochondrial genomes as a reference and found that the mitochondrial genome of *C. sabaeus* had the highest coverage and lowest divergence to the mitochondrial genome of Vero cells (Supplementary Table S2). Furthermore, a phylogenetic tree using whole mitochondrial genome

sequences indicated that the Vero cell line was closest to *C. sabaeus* (Fig. 2A). The gender of the AGM individual from which the Vero cell lineage was established has not yet been clearly described. A pair of X chromosomes in karyotyping (Fig. 1) and the almost diploid copy number of X chromosomes in sequence data (Fig. 2B) were observed in Vero JCRB0111 cells. Collectively, we concluded that the Vero cell lineage had been established from a female individual of *C. sabaeus*.

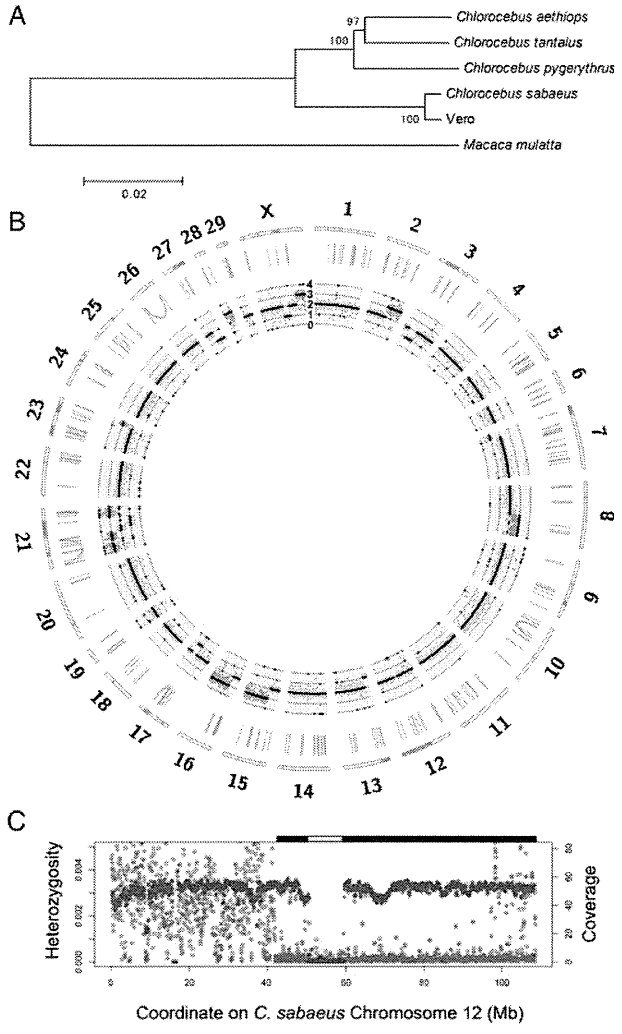

Figure 2. Genome landscape of the Vero genome. (A) Phylogeny of mitochondrial genomes of the Vero cell line, four *Chlorocebus* species, and *Macaca mulatta*. Bootstrap values with 1,000 replications were shown upon the branches. (B) Circos plot of the Vero cell genome. The orange bars in the outermost rectangles represent LOH regions. The blue, green, and orange lines in the middle layer show deletions, duplications, and inversions larger than 1 kb, respectively. The innermost plot shows the coverage of paired-end reads and expected ploidy (black lines). The blue, green, and orange dots represent the coverage values in 1×, 2×, and 3× regions, respectively. (C) The large deletion and LOH regions on *Chlorocebus sabaeus* chromosome 12. The red and blue points represent average heterozygosity (the number of heterozygous SNVs per bp) and genome coverage of paired-end reads in 1-Mb-size windows, respectively. The predicted homozygous deletion regions and LOH regions are shown as yellow and black bars on the plot area, respectively.

3.5. *Identification of SNVs*

To characterize SNVs in the Vero cell line nuclear genome, we mapped our paired-end reads to the reference genome of the rhesus macaque (*M. mulatta*), which has been annotated more than other non-human primate genome sequences. A total of 92% of the unambiguous sites of the rhesus macaque draft genome was covered with high-quality reads, and the genotype was called with high confidence (genotyping quality score $\geq$45 and coverage $\geq$10), which indicated that the rhesus macaque genome would work as a reasonable reference sequence for analysing the Vero cell genome. Approximately 58.5 million SNVs were identified (Supplementary Table S3). Of these, ~51.2 million and 7.3 million SNVs were homozygous and heterozygous, respectively. Most of the homozygous SNVs in the Vero cell line were attributed to evolutionary divergence between the genus *Macaca* and *Chlorocebus*, which was ~8–12 million years ago.[42,43] The estimated divergence between the rhesus macaque and Vero cell line genomes was ~2.2%. The level of heterozygous SNVs in the Vero cell line was also high and was markedly higher than that in a human individual.[44] This may be partly explained by the higher genetic diversity within AGM populations. We also identified ~2.9 and 2.7 million small deletions ($\leq$28 bp) and insertions ($\leq$44 bp), respectively (Supplementary Table S3).

3.6. *Detection of genomic rearrangements in the Vero cell line*

By comparing our paired-end reads with the publicly available draft genome of the AGM *C. sabaeus* (*C. sabaeus* 1.0: GCA_000409795.1), we examined potential >1- kb-scale deletions, segmental duplications, inversions, and translocations using the information of improper paired-end mapping and split-read mapping.[45] In order to present a landscape of genomic rearrangements in the main population of the Vero cell lines, we set stringent criteria for finding genome rearrangements that could identify rearrangements of high frequency in the cell population. A total of 138 deletions, 78 duplications, and 12 inversions of high frequency were detected (Fig. 2B; Supplementary Table S3), whereas none of the translocation candidates were detected at a high frequency. AGM chromosome 12 harboured a homozygous deletion that spanned across nearly 9 Mb (Supplementary Tables S3 and S4). The region was syntenic to human chromosome 9 and rhesus macaque chromosome 15 (from *MLLT3* to *LINGO2*) and contained ~40 genes including the type I interferon gene cluster and *CDKN2* genes (Fig. 2B

and C; Supplementary Table S4). This homozygous large deletion was validated as given below.

3.7. *Detection of LOH*

We identified copy number variations in different genomic regions using the mapping coverage of paired-end reads. Nine regions in chromosomes 2q, 8q, 15q, 16q, 21, 23q, 28, and Xq had three copies, while eight regions at 3p, 7p, 13p, 17q, 21q, 27q, and Xq were identified as a single copy (Fig. 2B). AGM chromosome 8p showed an intermediate coverage between two and three copies, in which the duplication and translocation of AGM chromosome 8p varied among the clones. These large-scale copy number changes agreed well with the karyotypes examined using M-FISH analysis (Fig. 1D). LOH regions were identified using the density of SNVs and its ratio to the density of homozygous SNVs. In addition to the identified haploid regions, we identified large LOH blocks in chromosomes 6q, 12q, and 23. The LOH on chromosome 12 harboured a large homozygous deletion (Fig. 2C; Supplementary Table S4; see also below).

3.8. *Validation of large deletions by PCR*

The large deletions predicted by the massively parallel sequencing system were validated by genomic PCR. Regarding the 8.85-Mb deletion of chromosome 12, a set of PCR primers striding across the deletion junction produced a ~230-bp amplicon from Vero cells, but not from normal AGM cells, while a PCR primer set designated for the AGM genome produced a predicted amplicon from normal AGM cells, but not from Vero cells (Fig. 3A). We tested two Vero cell lines, JCRB0111 and ATCC CCL81, and obtained identical results (Fig. 3A). In similar validation tests for another four large (>90 kb) predicted deletions (Supplementary Table S4), DNA fragments with breakpoint junctions were amplified from the Vero cell lines, but not from AGM PBMC for all these deletions, which confirmed the existence of these deletions in Vero cells (Fig. 3A; Supplementary Fig. S2). Four small (1–2 kb) predicted deletions were also confirmed to exist (Fig. 3B; Supplementary Fig. S2).

3.9. *Proviral SRV in the Vero JCRB0111 genome*

Analysis of collected SRV-related short reads from all paired-end short reads of the Vero JCRB0111 cell line, followed by analyses of gene assignment and long terminal repeat (LTR) finding, identified the 8,367 bp complete SRV genome sequence. The medians of variant frequencies were 25.5 and 8.0% in the highly variable and *env*-deleted region (nucleotide position 7525–7829) of SRV, respectively (Fig. 4). The copy number of SRV with 8.4-kb full length was estimated to be 30%, while that of SRV with the deletion of the 7525–7883 nucleotide (nt) region encompassing the C-terminal part in *env* and a portion of LTR was 70%. The SRV-Vero of JCRB0111 had 97% of the same nucleotides as those of ATCC CCL81 (Genbank_ID: JN134185). The number of minor alleles was 703 for SNVs and 1 for the insertion among the whole complete consensus SRV sequence in the Vero JCRB0111 genome. Four minor mutation sites caused three nonsense mutations and one frameshift on the *pol* or *env* region (Supplementary Table S5). Previous studies suggested a frameshift mutation in *pol* (position 3726) or frameshift mutation in *prt* (its position was not reported) on the SRV proviral sequences of Vero E6 or ATCC CCL81 cells.[46,47] However, our study did not detect equivalent mutations on the SRV proviral sequences of Vero JCRB0111 cells; however, other notable mutations were instead detected (Supplementary Table S5).

4. Discussion

By comparing with the AGM reference genome, the whole genome structure of Vero cells provided various important insights into the molecular characterization of this cell line. Vero cells are incapable of producing type I interferon in response to viral infections,[48] which may be the main cause for the high susceptibility of these cells to various types of microbes. The homozygous deletion of α- and β1-interferon genes in Vero cells was previously reported using classical DNA hybridization analysis.[49] The present study determined an ~9-Mb deleted region in chromosome 12 at the nucleotide level and further revealed an ~59-Mb LOH around the deleted region (Fig. 2B and C), which suggested that an ~9-Mb deletion first occurred in one of two homologous chromosome 12 during the establishment of cells, followed by a large-scale conversion that fixed the homozygous deletion of the region in the Vero cell lineage. The deleted region in chromosome 12 of Vero cells is syntenic to human chromosome 9p21–p22, which contains many genes of type I interferons (α8, α2, α1/13, α6, α14, α4, α17, α21, ω1, and β1) (Supplementary Table S4).

The human syntenic region corresponding to the deleted region in AGM chromosome 12 also contained *CDKN2A* and *CDKN2B*: *CDKN2A* encodes cyclin-dependent kinase (CDK) inhibitor 2A/p16^{INK4A} (which inhibits CDK6, a negative regulator of the retinoblastoma protein pRB) and p14^{ARF} (which inhibits the p53-negative regulator MDM2) in an alternate reading frame to the former, while *CDKN2B* encodes CDK inhibitor 2B/p15^{INK4B} (which inhibits another pRB-negative regulator CDK4) (Supplementary Table S4).[50,51] The CDK inhibitors and MDM2 inhibitor act as key regulators of the cell cycle, and mutations in *CDKN2A-CDKN2B* often occur in various types of human cancer; however, these mutations by themselves are not enough to transform

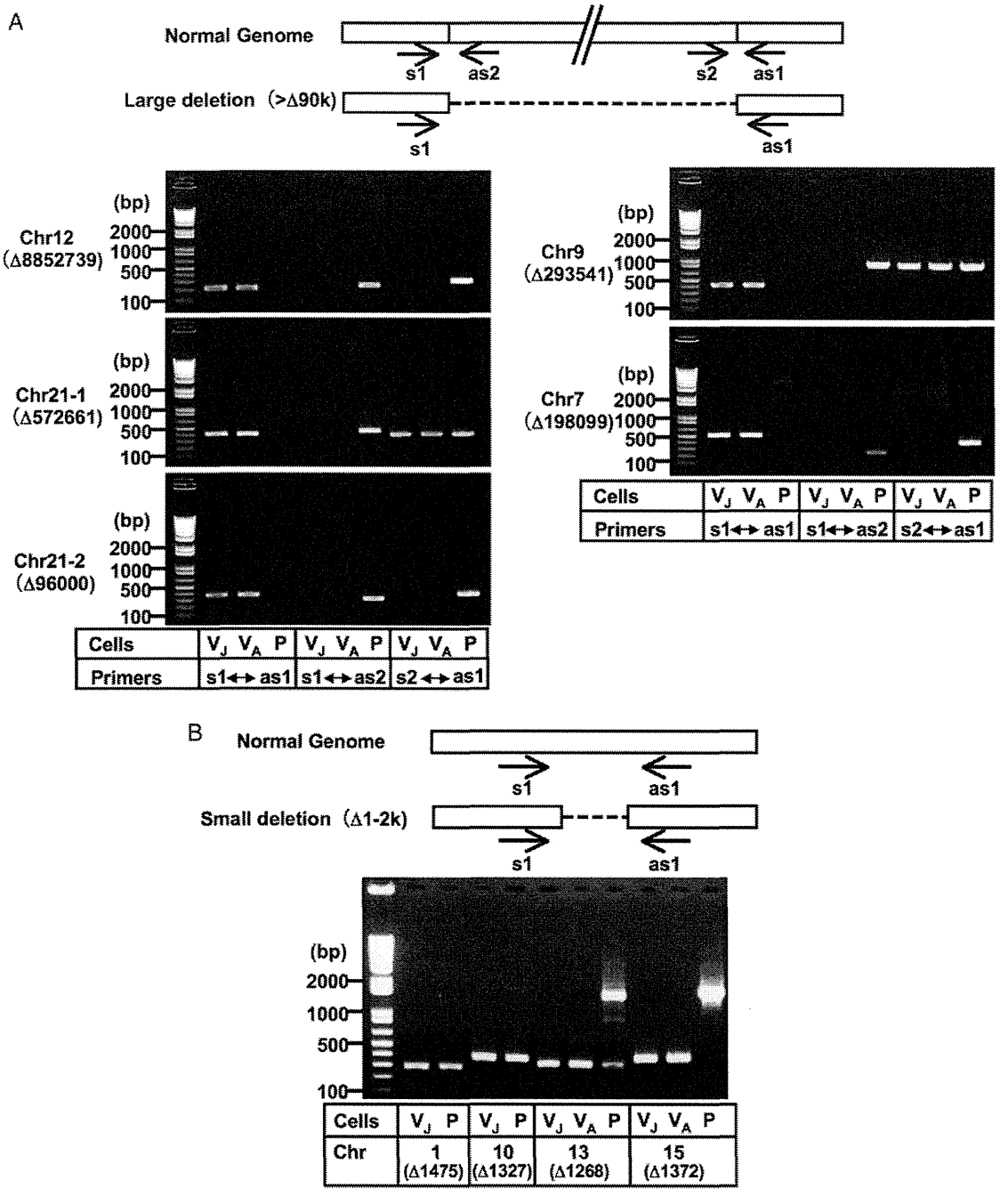

Figure 3. Validation of genomic deletions in Vero cells by PCR analysis. Large deletions (>90 kb deletions) (A) and some small deletions (1–2 kb deletions) (B) were selected. Although the genomic PCR confirmed the existence of breakpoint junctions for the 573 kb deletion in chromosome 21 and the 294 kb deletion in chromosome 9, a part of these regions appeared to exist somewhere in the genome (**A**; see also Supplementary Fig. S2). Amplicons corresponding to the deletions predicted in chromosomes 1 and 10 were produced not only from Vero cells, but also from AGM PBMC, while amplicons corresponding to the 'non-deleted' counterparts were not produced even from AGM PBMC (B; see also Supplementary Fig. S2), which indicated that our determined sequences for the Vero cell genome existed homozygously in these regions not only in Vero cells, but also in AGM PBMC. This paradox might be attributed to the possible incompleteness of the currently available version of the AGM whole-genome draft sequence or polymorphic state of the deletion within AGM populations. *Normal Genome* indicates the sequences predicted from the draft genome sequences of AGM and the rhesus macaque. Arrows indicate the primer positions used in the PCR analyses. The 'Δ' indicates the genomic deletion size predicted by the massively parallel sequencing system. The templates used were as follows: VJ, Vero JCRB0111; VA, Vero ATCC; P, AGM PBMC. PCR amplicons were sequenced to confirm the breakpoint sequences, which are shown in Supplementary Fig. S2. Chr, chromosome.

cells into tumourigenic cells.[50–52] The loss of both *CDKN2A* and *CDKN2B* may play a crucial role in the acquirement of immortality in the Vero cell lineage. Originally non-tumourigenic Vero cells may then acquire tumourigenicity when additional unknown mutations accumulate during prolonged passages.[15]

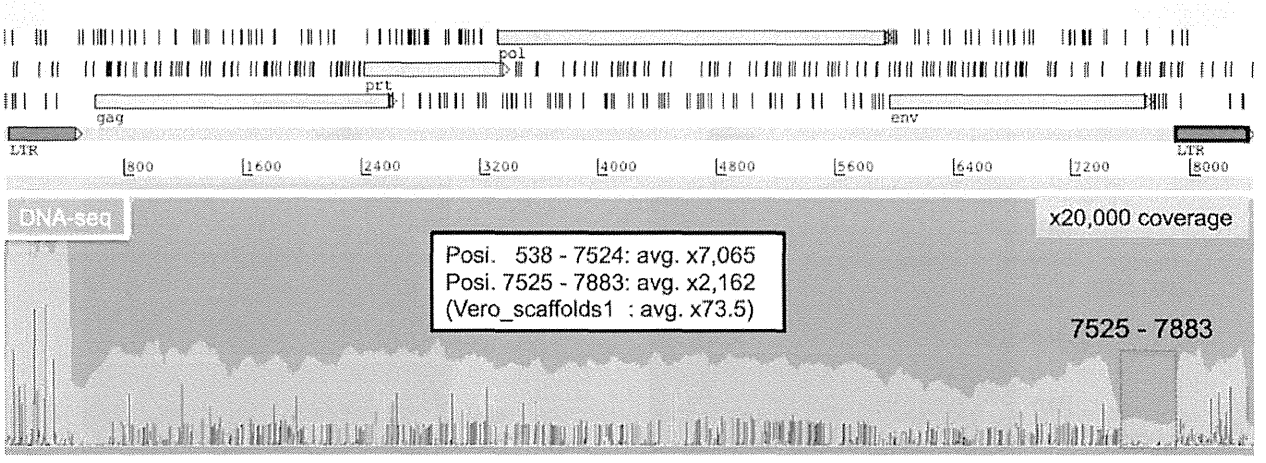

Figure 4. Characterization of proviral SRV sequences. DNA-seq short read mapping to the complete SRV-Vero genome sequence. Read depth and mismatch nucleotides are shown in the following colours (Depth: light grey, A: light green, T: red, G: orange, C: dark blue). The high variability of SRV sequences was rarely detected in the 7525–7883 nt region, whereas high variability was observed throughout other regions.

Although the karyological analysis demonstrated that Vero cells had various chromosomal rearrangements (Fig. 1C), no translocation was identified in the whole-genome sequence (Fig. 2B). This discrepancy may have been due to technical limitations. The karyotyping results obtained showed that most of the translocation events occurred between the telomeric regions of chromosomes, which could not be identified by sequencing if chromosomes fused via repeat sequences. In addition, in order to filter out rare chromosomal rearrangements in a cell population, events that occurred in only one of the homologous chromosomes may not be identified in our filtering criteria. Therefore, the absence of translocation rearrangements by sequencing does not contradict the results of the karyological analysis, which showed that all or most chromosomal translocations were observed in one of the two homologous chromosomes (Fig. 1C and D; Supplementary Fig. S1C and D). Haplotype sequencing may be necessary to determine such heterozygous events.

Many SRV sequence variations existed in Vero JCRB0111 cells (Fig. 4). As for SRV associated with the vaccine-producing Vero E6 cell line (the parental cell line of which is ATCC CCL81), a frame-shifting single-nucleotide insertion in the polymerase gene was identified.[46] This frameshifting mutation was not detected in SRV associated with the Vero ATCC CCL81 cell line[47] or Vero JCRB0111 cell line (this study). SRV variant sequences lacking the U3 and R regions of 3′LTR were instead detected in Vero ATCC CCL81-associated SRV,[47] while the results of this study suggested that some SRV copies in the Vero JCRB0111 cell genome were defective in the *env*-3′LTR region (Fig. 4). Thus, a large amount of diversity may occur in proviral SRV sequences during the passage of Vero cells.

Various quality tests must be conducted in order to fully characterize cell banks for pharmaceutical use[53] (The WHO guidelines on animal cell substrates are available at http://www.who.int/biologicals/vaccines/TRS_978_Annex_3.pdf.) Many of these tests rely on conventional methodology, and some tests still use many experimental animals. The whole-genome sequence should be invaluable reference information to develop more rational and effective methods for identification, genetic stability, and microbial agents in pharmaceutical cell banks. For example, the currently authorized tests for cell identity consist of classical methods (e.g. isoenzyme analysis and G-band analysis) and more modern DNA profiling methods (e.g. restriction fragment length polymorphism and variable number of tandem repeats analysis). These tests, even if not all, require a considerable amount of time and money as well as well-trained technical skills, and some are not accurate enough to discriminate different cell lines established from the same biological species. This study presented a proof of the concept that PCR analysis will open a rapid and accurate alternative method for the cell identity test to detect unique chromosomal deletions (Fig. 3). Metagenome analysis is a powerful approach that can be used to survey microbial contamination in biological pharmaceuticals.[46,47,54] This study also employed DNA-seq short reads of Vero cell genome DNA to comprehensively survey microbe-related sequences in the cell sample, and detected no discernible sign of microbe-relevant sequences (except for endogenous SRV) in Vero JCRB0111 cells. In this direction, it is crucial to distinguish between endogenous and exogenous viral-like sequences, because the appearance of the former is inevitable and can serve as an internal positive control in metagenomic analysis for microbial agents. In addition, the heterogeneity in SRV sequences as discussed above may also be a good genomic signature for identifying a specific cell seed among various Vero cell sub-lines. The whole-genome